Expected and Unexpected Imaging Findings after ^{90}Y Transarterial Radioembolization for Liver Tumors

Juan C. Spina, MD
Isabel Hume, MD
Ana Pelaez, MD
Oscar Peralta, MD
Marcos Quadrelli, MD
Ricardo Garcia Monaco, MD

Abbreviations: ADC = apparent diffusion coefficient, FDG = fluorine 18 fluorodeoxyglucose, HCC = hepatocellular carcinoma, LSF = lung shunt fraction, MAA = macroaggregates of human serum albumin, REILD = radioembolization-induced liver disease, TARE = transarterial radioembolization

RadioGraphics 2019; 39:578–595

https://doi.org/10.1148/rg.2019180095

Content Codes: GI IR VA

From the Departments of Radiology (J.C.S., A.P., O.P., M.Q., R.G.M.) and Nuclear Medicine (I.H.), Hospital Italiano, Tte Gral Juan Domingo Perón 4230, C1199ABH CABA, Buenos Aires, Argentina. Presented as an education exhibit at the 2017 RSNA Annual Meeting. Received March 18, 2018; revision requested May 24 and received June 18; accepted June 21. For this journal-based SA-CME activity, the authors, editor, and reviewers have disclosed no relevant relationships. **Address correspondence to** J.C.S. (e-mail: *juan.spina@hospitalitaliano.org.ar*).

SA-CME LEARNING OBJECTIVES

After completing this journal-based SA-CME activity, participants will be able to:

- Describe the fundamentals of the ^{90}Y TARE procedure.
- Discuss the roles of CT and MRI in the evaluation of treatment response.
- Identify characteristic imaging findings and complications seen during the follow-up after TARE.

See rsna.org/learning-center-rg.

Transarterial radioembolization (TARE), also called radioembolization or selective internal radiation therapy, is an interventional radiology technique used to treat primary liver tumors and liver metastases. The aim of this therapy is to deliver tumoricidal doses of radiation to liver tumors while selecting a safe radiation dose limit for nontumoral liver and lung tissue. Hence, correct treatment planning is essential to obtaining good results. However, this treatment invariably results in some degree of irradiation of normal liver parenchyma, inducing different radiologic findings that may affect follow-up image interpretation. When evaluating treatment response, the treated area size, tumor necrosis, devascularization, and changes seen at functional MRI must be taken into account. Unlike with other interventional procedures, with TARE, it can take several months for the tumor response to become evident. Ideally, responding lesions will show reduced size and decreased enhancement 3–6 months after treatment. In addition, during follow-up, there are many imaging findings related to the procedure itself (eg, peritumoral edema, inflammation, ring enhancement, hepatic fibrosis, and capsular retraction) that can make image interpretation and response evaluation difficult. Possible complications, either hepatic or extrahepatic, also can occur and include biliary injuries, hepatic abscess, radioembolization-induced liver disease, and radiation pneumonitis or dermatitis. A complete understanding of these possible posttreatment changes is essential for correct radiologic interpretations during the follow-up of patients who have undergone TARE.

Introduction

Transarterial radioembolization (TARE) is an interventional radiology technique used to treat patients with primary liver tumors and liver metastases. It is also called radioembolization or selective internal radiation therapy. This procedure involves delivering glass or resin microspheres loaded with yttrium 90 (^{90}Y) through a catheter into the artery or arteries supplying target lesions. It was first described as a procedure without severe complications by Herba et al in 1988 (1).

^{90}Y is a high-energy β-particle emitter with a half-life of 64.053 hours. The principal decay mode is negatively charged β-particle emission that leads to the decay of ^{90}Y to stable zirconium 90. The mean and maximal depths of ^{90}Y penetration into soft tissue are 2.5 and 11.0 mm, respectively. Unlike with external radiation therapy, with TARE, the delivery of microspheres closer to the target lesion allows very high doses to be used, with less toxicity to the adjacent liver parenchyma (2,3).

TEACHING POINTS

- During follow-up, there are many imaging findings related to the TARE procedure itself that can make image interpretation and response evaluation difficult. Among such findings, the most frequent are peritumoral edema, inflammation, ring enhancement, hepatic fibrosis with portal hypertension, and capsular retraction.
- Performing ^{99m}Tc-MAA SPECT/CT is useful for identifying extrahepatic visceral sites that are at risk for postradioembolization complications because it increases the sensitivity and specificity of ^{99m}Tc-MAA SPECT.
- Early (before 30 days) follow-up after TARE can lead to erroneous interpretations because necrosis, hemorrhage, and edema or inflammation initially can induce an apparent increase in tumor lesion size. Hence, tumor response evaluation must be performed after 3 months.
- It may take 2–3 months before tumor size changes are observable with cross-sectional imaging methods; however, early response can be assessed by using diffusion-weighted imaging. The ADCs of responding primary tumors and liver metastases increase after treatment, reflecting a decrease in tumor cellularity.
- Complete peritumoral ring enhancement after TARE is indicative of a good response with no viable tumor.

SIR-Spheres (Sirtex Medical, North Sydney, Australia) and TheraSpheres (Nordion, Ottawa, Ont, Canada) are the two microspheres that are currently available for clinical use. SIR-Spheres are nondegradable ^{90}Y-loaded resin microspheres that range in diameter from 20 to 60 mm. TheraSpheres are ^{90}Y-incorporated glass microspheres that are 20–30 mm in diameter (4). These microspheres will remain permanently implanted within the vasculature of tumors, delivering a lethal selective radiation dose of β-particle emissions to tumor tissue while minimizing the irradiation of surrounding tissues.

In contrast to healthy liver parenchyma, which obtains its blood supply mainly from the portal venous circulation, primary and secondary hepatic tumors are vascularized mainly by arterial blood flow, and with TARE, one takes advantage of this factor (5). Even hepatic metastatic lesions larger than 3 mm receive 80%–100% of their blood supply from the hepatic arterial circulation rather than the portal venous circulation (6). This predominance of arterial blood supply to hepatic tumors allows the preferential deposition of microspheres into tumors rather than normal parenchyma, maximizing tumor irradiation (7,8). A high radiation dose is delivered to the tumor capillary bed, resulting in cellular death and tumor necrosis, while the liver parenchyma is relatively preserved (9). Acute and subacute toxic effects from TARE are more tolerable than are the toxic effects associated with other hepatic embolization procedures (7).

Patient selection for TARE includes assessments of the disease burden, biochemical profile, and patient performance status (10). Procedure planning includes performing multidetector CT or MRI for assessment of the liver lesions and arterial mapping. This planning also requires a pretreatment simulation examination that includes hepatic angiography and technetium 99m (^{99m}Tc) macroaggregated human albumin (MAA) nuclear scanning (11). The goal in using this treatment is to induce tumor necrosis with size reduction; however, response assessment is challenging. Tumor size determinations can be misleading owing to the therapy-induced transformation of tumor into necrosis or fibrosis (12). In fact, after TARE, the tumor size may decrease, remain stable, or even increase. Therefore, treatment response should be evaluated by using, in addition to standard size criteria, other findings such as tumor necrosis, reduction in tumor vascularity, variation in fluorine 18 fluorodeoxyglucose (FDG) uptake at PET, and changes in signal intensity at diffusion-weighted MRI (6).

In addition, during follow-up, there are many imaging findings related to the TARE procedure itself that can make image interpretation and response evaluation difficult. Among such findings, the most frequent are peritumoral edema, inflammation, ring enhancement, hepatic fibrosis with portal hypertension, and capsular retraction. Complications of TARE also are possible and include biliary necrosis, biloma, hepatic abscess, and radioembolization-induced liver disease (REILD). Extrahepatic complications (ie, radiation-induced cholecystitis, pneumonitis, or dermatitis) are unusual but occur in a minority of cases.

The combined effects of embolization and radiation induce lesional and perilesional changes that can be different from and more variable than the lesional and perilesional changes seen with other transarterial procedures. Hence, a complete understanding of these possible posttreatment changes is essential for correct radiologic interpretations during the follow-up of patients who have undergone TARE. In this article, we describe the TARE procedure, posttreatment evaluation, and most frequent findings and complications that can be detected during follow-up imaging.

Treatment Planning and Mapping

TARE is effective when delivered at the right location, with the right radiation dose, and with the right intent (13). The aim of this therapy is to deliver tumoricidal doses of radiation to liver lesions, regardless of their number, size, and location (13,14), while selecting a safe radiation

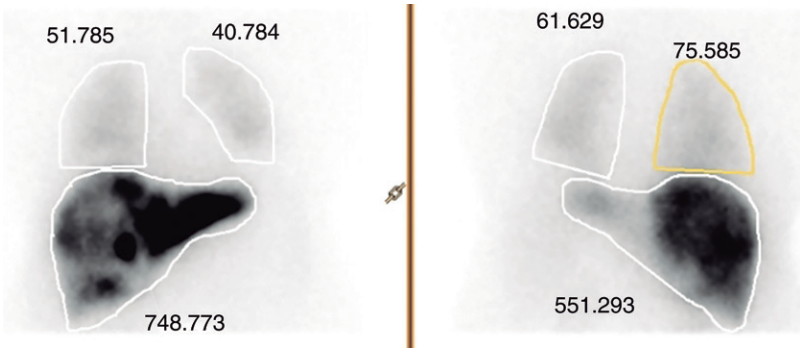

Figure 1. Hepatopulmonary shunt fraction quantification. The lung shunt fraction *(LSF)* is calculated at planar ^{99m}Tc-MAA scintigraphy by using regions of interest drawn on static anterior and posterior scans of the thorax and abdomen. The LSF in this case is 14%.

dose limit for normal (nontumoral) liver and lung tissue. Hence, accurate treatment planning is essential to obtaining good results. However, despite all precautions, some degree of irradiation to normal liver parenchyma may occur (15).

Therapy planning includes a pretreatment simulating phase, the purposes of which are detection of excessive hepatopulmonary shunting, mapping of tumor-perfusing vessels, and identification of vessels that could deliver microspheres to nontargeted organs such as the stomach, gallbladder, duodenum, and pancreas and thus lead to complications. Nontargeted sites of delivery can be safely bypassed with use of transcatheter embolization. The presence of extrahepatic vasculature that cannot be corrected by using angiographic techniques (embolization or placement of the catheter distal to these vessels) may exclude the patient from treatment. Because these vessels can revascularize, the treatment should be performed as closely as possible to the intended time of treatment.

Because ^{90}Y is a pure β-particle emitter, the pretreatment angiographic procedure (ie, mapping) is performed with ^{99m}Tc-MAA. MAA particles are 30–90 μm in diameter, similar in diameter to the ^{90}Y microspheres but not identical in size and shape. Before the injection of ^{99m}Tc-MAA, the syringe should be tilted to agitate and resuspend the particles; this will minimize clumping of the particles, which can lead to heterogeneous distribution (4). The injected dose is typically 185 MBq (5 mCi) suspended in normal saline solution (4,16).

One source of interpretation error may be free pertechnetate, especially if activity is observed in the stomach, where it is difficult to distinguish free pertechnetate from incorrectly administered tracer. Visibility of the thyroid, stomach, and urinary bladder enables one to determine the qualitative degree of circulating free pertechnetate (15). To prevent the concentration of dissociated ^{99m}Tc-pertechnetate, ^{99m}Tc-MAA should be prepared by using quality control assessments with high labeling efficiency, and the delay in imaging after the endovascular procedure should be minimized (17). Scintigraphy should be performed within 1 hour of the ^{99m}Tc-MAA injection to avoid in vivo degradation of the ^{99m}Tc-MAA particles (4). Free ^{99m}Tc is normally observed as diffuse stomach uptake, whereas disease-related uptake is seen as focal uptake (15,18). At some centers, 600 mg of perchlorate is administered 30 minutes before angiography is performed (17,19).

In the nuclear medicine department, γ-camera ^{99m}Tc-MAA scintigraphy should be performed to analyze the MAA distribution pattern. Static images of the thorax and abdomen in the anterior and posterior projections are obtained; then SPECT/CT of the abdomen is performed with a low-energy, thin-section collimator.

The essential purposes of obtaining these images are *(a)* assessment of pulmonary shunting (hepatopulmonary shunt fraction quantification), *(b)* assessment and ruling out of extrahepatic uptake, and *(c)* determination of the optimal therapeutic activity to be deposited.

Hepatopulmonary Shunt Fraction Quantification

Lung shunting could result in radiation pneumonitis after the administration of ^{90}Y. Therefore, during treatment planning, lung shunting should be detected and quantified (15) for estimation of the percentage of ^{90}Y that bypasses the liver and enters the lungs.

Regions of interest are manually drawn around the lungs and liver. The percentage of lung shunting can be calculated from the total counts within the region of interest of both lungs and liver by using the geometric mean of anterior and posterior thoracic and abdominal planar images (Fig 1).

The estimated LSF without attenuation correction is a large overestimation compared with attenuation-corrected measurements (15). LSF estimation is reproducible, and interobserver variability seems to be small. Scans of suboptimal quality due to tracer degradation (visualization

of stomach, thyroid, or kidneys) correlate with higher LSF (15,16).

For resin microspheres, patients with LSFs higher than 10% require radiation dose reductions, as recommended by the manufacturer. In patients with LSFs of 10%–15%, the amount of SIR-Spheres delivered should be reduced by 20%. In patients with LSFs of 16%–20%, the amount delivered should be reduced by 40%. Patients with LSFs higher than 20% should not be injected with SIR-Sphere microspheres (20). The results of previous preclinical and clinical studies of ^{90}Y microspheres have shown the highest tolerable accumulated dose to the lungs to be up to 30 Gy in a single injection or 50 Gy over multiple injections (19,21).

Fused SPECT/CT

Identifying the uptake of ^{99m}Tc-MAA in sites other than the liver is a crucial part of the therapeutic management of patients because inadvertent delivery of ^{90}Y microspheres outside the liver into the gastroduodenal tract or gastric circulation may have grave clinical consequences such as ulceration, bleeding, and/or pancreatitis. Planar imaging analysis can lead to misinterpretation of the extrahepatic uptake due to low spatial resolution. Foci of ^{99m}Tc-MAA adjacent to or at the edge of the liver and upper abdomen in particular may be difficult to detect as extrahepatic sites owing to organ superpositioning mainly in a heterogeneous ^{99m}Tc-MAA distribution.

If extrahepatic uptake is detected, anatomic localization of the foci can help the radiologist identify the culprit vessel. This localization is greatly facilitated by the use of fused SPECT/CT images (Fig 2). Performing ^{99m}Tc-MAA SPECT/CT is useful for identifying extrahepatic visceral sites that are at risk for postradioembolization complications because it increases the sensitivity and specificity of ^{99m}Tc-MAA SPECT. As has been demonstrated in retrospective and prospective studies (18,22,23), SPECT/CT enables identification of the inadvertent extrahepatic deposition of ^{99m}Tc-MAA activity more accurately than does SPECT or planar imaging alone, which allows direct correlation of anatomic and scintigraphic information only.

Empirical and Dosimetric Assessment of Treatment Activity

Different methods are used to determine treatment activity. Empirical and dosimetric methods (24) are described in user manuals (20).

Empirical Methods.—With the empirical method, a standard amount of radioactivity based on the tumor burden in the liver is recommended. For tumor involvement of more than 50% of the liver, 3.0 GBq of activity is recommended; for 25%–50% tumor involvement, 2.5 GBq is recommended; and for less than 25% tumor involvement, 2.0 GBq is recommended. The empirical method of determining treatment activity has been replaced with the body surface area method.

The body surface area method is a variant of the empirical method. In this method, the body surface area calculated from the patient's weight and height is incorporated with the percentage of involved liver (tumoral and nontumoral) calculated with CT or MRI.

Dosimetric Methods.—There are two dosimetric methods of determining treatment activity: noncompartmental MIRD (medical internal radiation dose) macrodosimetry, for use with the glass spheres (ie, TheraSpheres), and compartmental MIRD macrodosimetry, which can be used with the glass and resin (ie, SIR-Spheres) spheres (15,24). With the MIRD method, the tumor-to-nontumor tissue ratio is used to express the relative distribution of ^{99m}Tc-MAA by determining the areas of interest in healthy and tumoral liver tissue at SPECT image acquisitions. The aim is to deliver a tumoricidal dose to the tumor while preserving safe limits of radiation to normal liver parenchyma and the lungs. The recommended safe dose limits are 70 Gy for nontumoral liver tissue (<50 Gy in cirrhotic livers) and 30 Gy for the lungs in a single injection, or 50 Gy in subsequent treatments. However, these limits need to be confirmed in prospective studies (12,13). The safety dose for tumoral liver tissue has no upper limit.

In daily practice, the body surface area method is the most commonly applied when the resin microspheres are used. Nonetheless, the partition model based on pretreatment ^{99m}Tc-MAA scan findings should be preferred because lesion-based dosimetric results have been shown to correlate with treatment response and survival (11,17,18).

Cone-Beam CT

In cone-beam CT, a rotational C-arm equipped with an x-ray source and flat panel detector encircles the patient, as part of the angiography suite. Use of a C-arm enables the acquisition of intratreatment CT images and three-dimensional vascular images to improve the detection of catheter positioning, tumor feeding vessels and hepatic or extrahepatic feeding vessels, extrahepatic enhancement, and incomplete tumor perfusion, and improve the assessment of procedure technical success (25) (Fig 3).

Louie et al (26) described a modification of their treatment plan, owing to the detection of extrahepatic enhancement or incomplete tumor

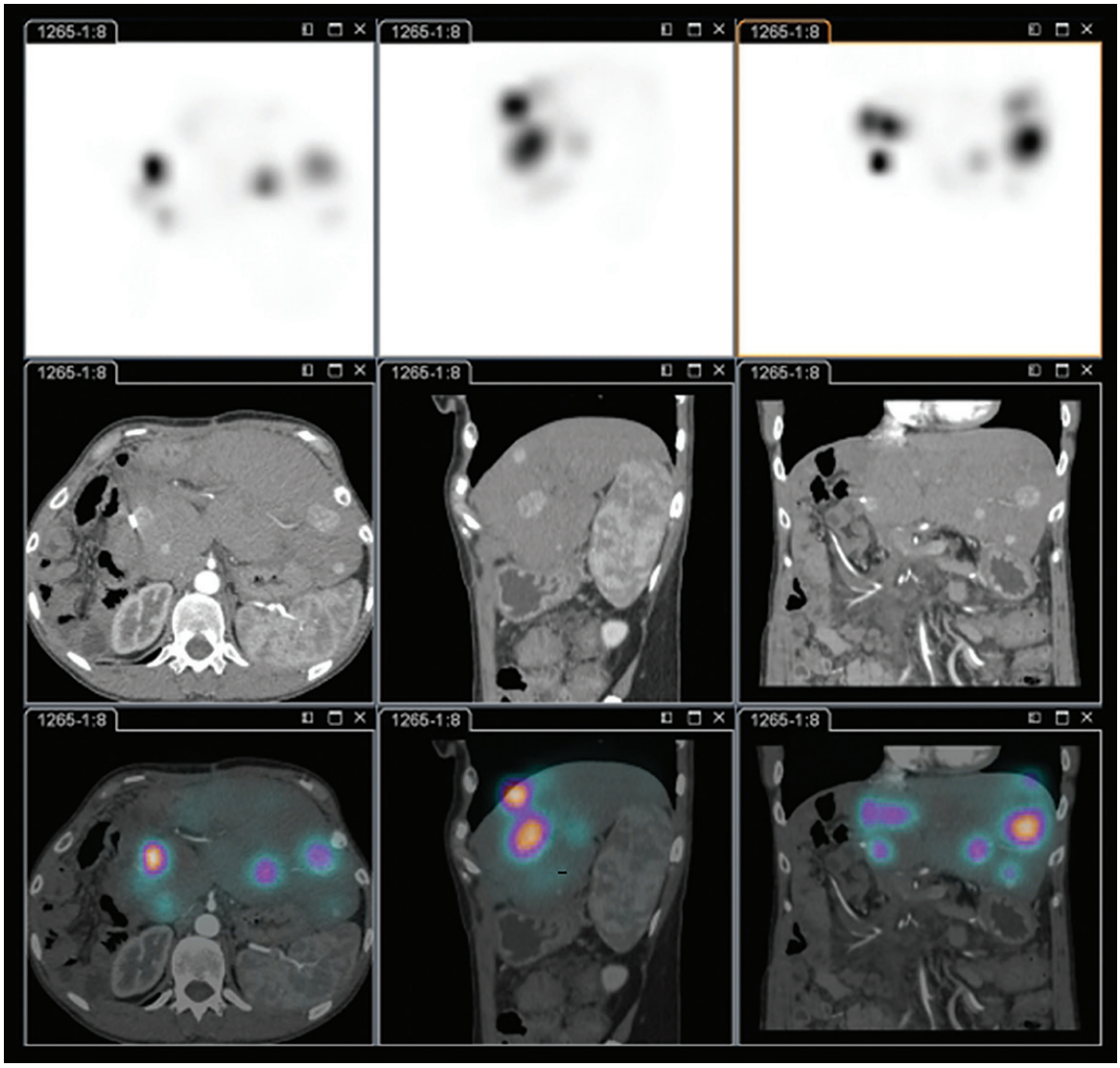

Figure 2. ^{99m}Tc-MAA uptake in liver tumors in a 42-year-old woman. Axial (left), sagittal (middle), and coronal (right) SPECT (top row), CT (middle row), and fused SPECT/CT (bottom row) images show several liver tumors. The SPECT/CT images show high intratumoral uptake of ^{99m}Tc-MAA in the liver lesions (round colored regions) and minimal uptake in the normal (noncolored) liver parenchyma.

perfusion, in 52% of cases when cone-beam CT was used. Cone-beam CT findings directed the additional embolization of vessels or the repositioning of the catheter for better contrast agent and microsphere distribution. Louie et al (26) concluded that cone-beam CT can provide additional information about tumor and tissue perfusion that is not currently detectable at digital subtraction angiography or ^{99m}Tc-MAA imaging, optimizing ^{90}Y microsphere delivery and reducing nontarget embolization.

Assessment of Postprocedural Technical Success and Treatment Response

There are two methods for assessing technical success immediately after the TARE procedure: bremsstrahlung SPECT/CT (27) and ^{90}Y PET/CT. These examinations are performed to visualize the distribution of ^{90}Y activity and verify that there are no ^{90}Y microspheres in organs other than the liver. ^{90}Y PET/CT is also useful for postdosimetric calculations (28,29) (Fig 4).

Specific problems in the evaluation of treatment response after local-regional treatment of liver lesions with TARE are related to the tumor type, injection flow and time of image acquisition, local-regional treatment, and number of embolizations performed. In terms of tumor type, hypervascular (hepatocellular carcinoma [HCC], neuroendocrine metastases) versus hypovascular (eg, colorectal liver metastases, cholangiocarcinoma) tumor lesions have different patterns of enhancement at pretreatment evaluation.

The injection flow and time of image acquisition after the injection (arterial, portal venous,

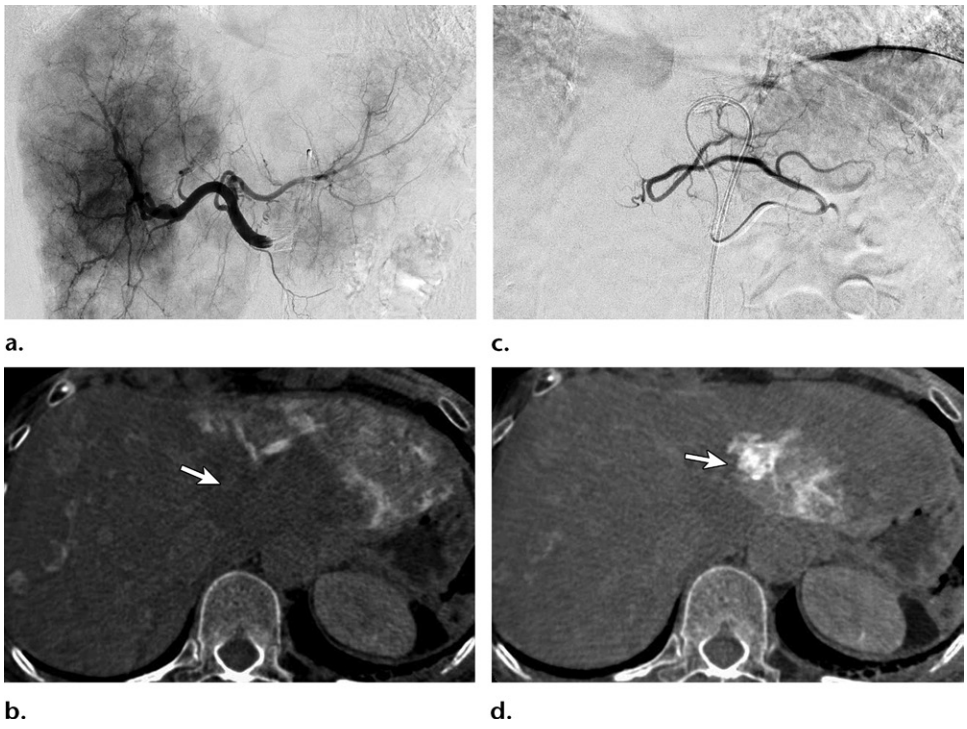

Figure 3. Vascular planning and mapping before treatment of bilateral hepatic metastases of pancreatic neuroendocrine tumor. **(a)** Hepatic angiogram shows the liver arterial supply; the segment II artery is not visualized. **(b)** Axial cone-beam CT image obtained during contrast agent injection in the segment III artery shows a lack of enhancement (arrow) in the medial portion of the targeted left tumor. **(c)** Left gastric angiogram shows the origin of the segment II artery, vascular supply of that segment, and missing sector of the left tumor. **(d)** Axial cone-beam CT image obtained during selective contrast agent injection in the segment II artery better depicts the missing sector of the left targeted tumor (arrow). This image does not show stomach enhancement and thus enables safe injection of the ^{90}Y spheres.

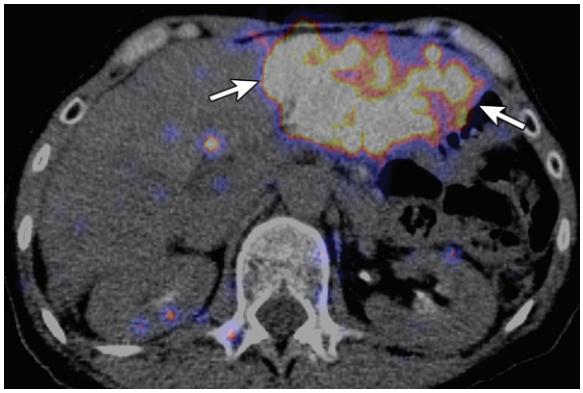

Figure 4. Assessment of technical success after ^{90}Y-sphere embolization in the same patient as in Figure 3. ^{90}Y PET/CT image obtained immediately after split ^{90}Y infusion in liver segments II and III shows homogeneous radiopharmaceutical uptake in the targeted tumor (arrows) and a lack of extrahepatic uptake.

or delayed phase) can influence the identification and size of nontreated lesions (at baseline examination) and treated lesions (during follow-up). The phase during which the lesions are most visible may vary as a result of the treatment. On the other hand, apparent new lesions may appear after treatment owing to their better visibility as a result of devascularization. This problem is less evident on MR images because the lesions can often be measured by using MRI sequences without contrast material injection (30).

Local-regional treatments induce morphologic changes (eg, devascularization, necrosis), so their effectiveness cannot be assessed on the basis of lesion size alone (30). Finally, not all liver lesions can be effectively treated during one procedure, so radiologists must perform correct mapping of the treated lesions before reporting the treatment response.

The recommended times for obtaining posttreatment images and performing laboratory evaluation are not fully agreed on. In the study by Riaz et al (11), triphasic CT or MR images were obtained 1 month after treatment and at 3-month intervals following the first posttreatment evaluation, as it may take 3–6 months for the optimal response (ie, size reduction) to occur.

Tumor Size, Necrosis, and Pseudoprogression

With transarterial chemoembolization, the goal of treatment is to induce tumor necrosis despite absent or nonapparent tumor shrinkage, and a good response to tumor devascularization can be detected soon after treatment, at 1 month follow-up. In contrast, the radiologist must cautiously

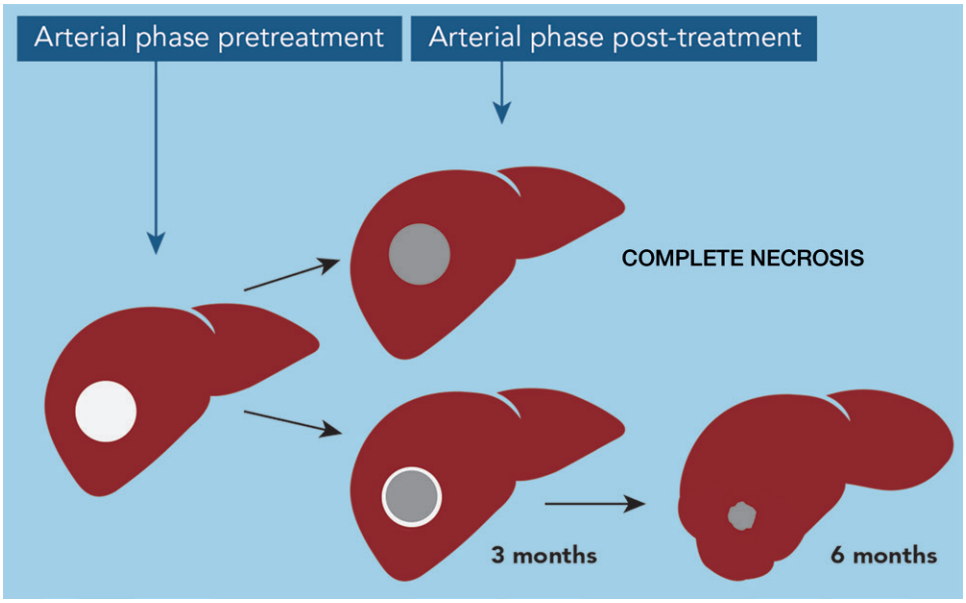

Figure 5. Illustration demonstrates complete tumor response after TARE. Complete tumor response may involve complete necrosis or progressive devascularization and a decrease in size over time. Sometimes ring enhancement may appear. Atrophy of the treated lobe, as depicted here, also can occur.

interpret the treatment response after TARE, because this can take several months to manifest according to traditional anatomic criteria (Figs 5, 6).

Responding lesions ideally will show a reduction in size and decreased enhancement at 3–6 months (Fig 7). Many patients demonstrate necrosis and/or peritumoral edema or inflammation, which can lead to an underestimation of the treatment response or an overestimation of tumor progression (Fig 8). In some cases, stable or even increased tumor size (pseudoprogression), with reduced blood flow to the tumor mass, is reported, probably owing to tumor necrosis, hemorrhage, or edema. Pseudoprogression without enhancement has been reported to appear a mean of 29–31 days after TARE and may persist for several months (6).

Early (before 30 days) follow-up after TARE can lead to erroneous interpretations because necrosis, hemorrhage, and edema or inflammation initially can induce an apparent increase in tumor lesion size. Hence, tumor response evaluation must be performed after 3 months. New foci also may be observed at posttreatment follow-up owing to their increased visibility following the devascularization of lesions (Fig 9). Knowledge of the described posttreatment findings is important because lesion stability or increased lesion size may be misinterpreted by the reading radiologist as disease progression and thus affect patient management.

Treatment Response of HCC and Hypervascular Metastases

Since 2000, the European Association for the Study of the Liver and the American Association for the Study of Liver Disease have endorsed criteria related to changes in only the viable portion of tumors, defined as the portion with enhancement after injection during the arterial phase, for assessment of the effectiveness of local therapies (30). Along these same lines, in 2010 Lencioni and Llovet (31) proposed a modified version of the Response Evaluation Criteria in Solid Tumors (RECIST) guidelines in which tumor necrosis is designated a treatment effect. According to the revised criteria, the response of target lesions is evaluated by using the percentage change in the sum of the diameters of the viable portions and can be reported as a complete response (ie, disappearance of any intratumoral arterial enhancement in all target lesions), partial response (>30% decrease in the sum of the diameters of viable target lesions), progressive disease (>20% increase in the sum of the diameters of viable target lesions), or stable disease (30,31). The modified RECIST (mRECIST) guidelines are currently the most widely used criteria for evaluating the treatment response in patients with HCC. Similar criteria can be used to assess the treatment response of other hypervascular tumors such as neuroendocrine liver metastases.

Some authors propose using the Choi criteria (32,33) with multidetector CT to assess treatment response. These criteria were originally created to evaluate gastrointestinal tumors, but they may be adopted for assessment of other tumors. With these criteria, partial response is defined as a 10% reduction in the size or 15% reduction in the attenuation of the treated lesions during the portal venous phase (32,33).

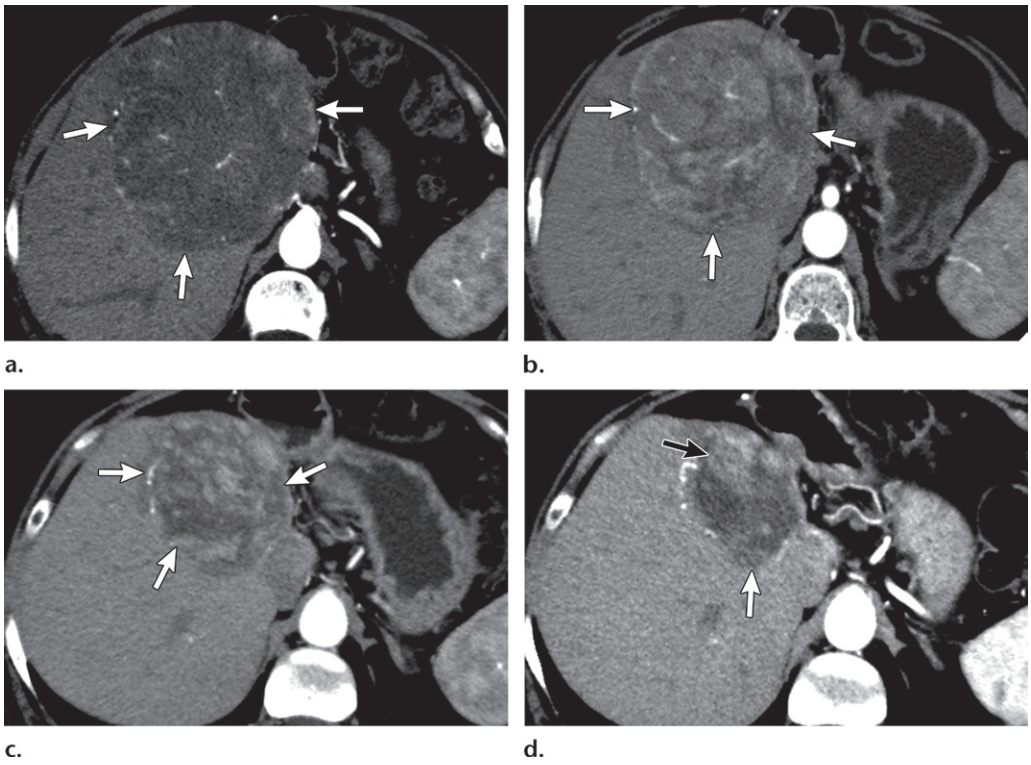

Figure 6. Axial arterial phase CT findings before and after TARE in a 67-year-old woman who had cirrhosis and HCC. **(a)** Contrast material–enhanced pretreatment image shows HCC (arrows) in liver segments IV, VII, and VIII. **(b)** Image obtained 45 days after treatment shows the lesion (arrows) with a stable size and persistent enhancement. **(c, d)** Images obtained 3 months **(c)** and 6 months **(d)** after treatment show a progressive reduction in tumor size and partial devascularization of the lesion (white arrows), with residual enhancement (black arrow in **d**) in the anterior sector.

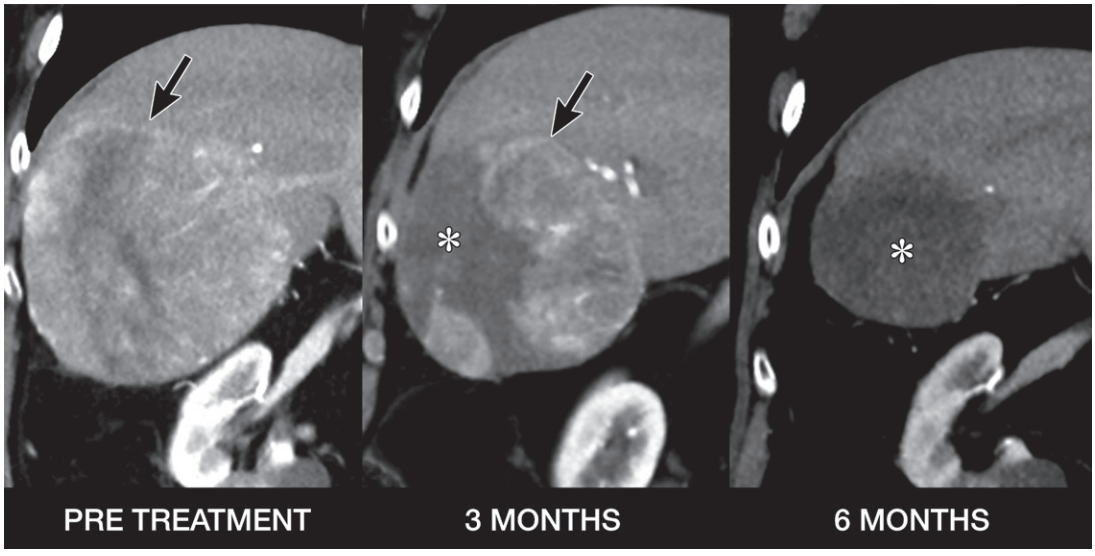

Figure 7. Coronal arterial phase CT images show tumor responses after TARE in an 80-year-old man. Left: Image obtained before TARE shows cirrhosis and HCC (arrow) in liver segments V–VIII. Middle: Image obtained 3 months after treatment shows a partial tumor response, with necrosis (*) and residual enhancement (arrow). Right: Image obtained 6 months after treatment shows complete necrosis (*).

Treatment Response of Liver Metastases and Hypovascular Tumors

The most widely accepted set of guidelines for assessing treatment response in clinical trials is RECIST version 1.1, which is based on changes in tumor size (34) and can be adopted for patients with hypovascular tumors and liver metastases. The definition of partial response is a greater than 30% reduction in the sum of the longest cross-sectional diameters of the treated lesions.

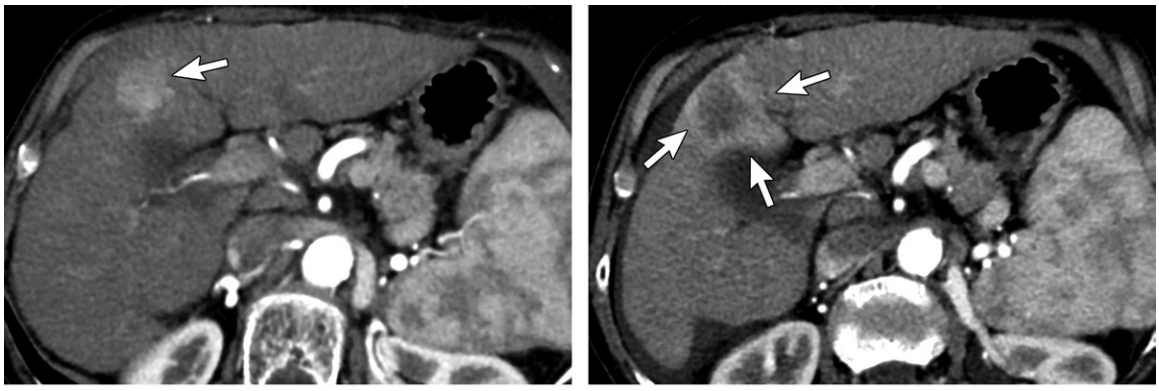

a. b.

Figure 8. Peritumoral edema and inflammation in a 78-year-old woman with liver cirrhosis. **(a)** Axial pretreatment arterial phase CT image shows HCC (arrow) in liver segment IV. **(b)** Axial arterial phase CT image obtained 3 months after treatment shows an apparent increase in size, with perilesional enhancement due to parenchymal inflammation (arrows).

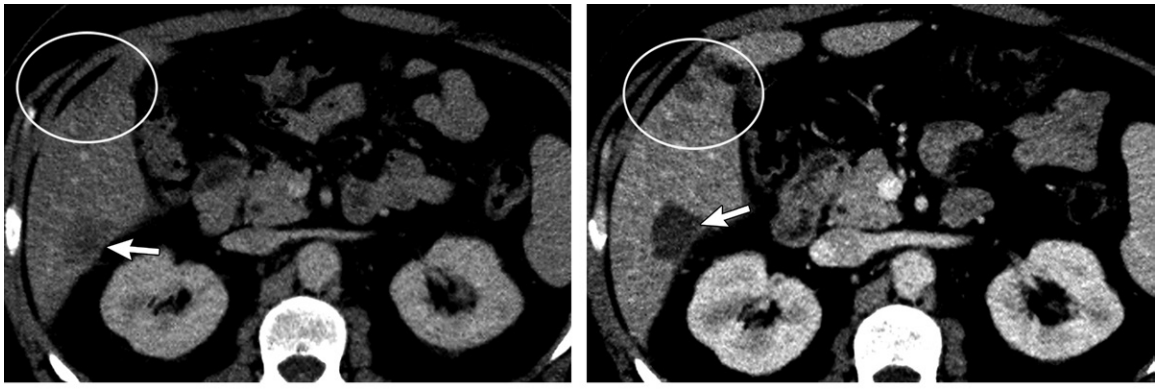

a. b.

Figure 9. Pseudoprogression of disease in a 60-year-old man with colorectal liver metastases. **(a)** Axial portal venous phase CT image shows liver metastasis (arrow) in liver segment VI. **(b)** Axial posttreatment portal venous phase CT image shows an apparent new lesion (circle) in liver segment V caused by devascularization of a lesion that was poorly seen (circle in **a**) at pretreatment CT. Note the complete necrosis (arrow) of the segment VI metastasis after treatment.

However, a partial response can be achieved without an evident reduction in lesion size. Tochetto et al (9) found that a 15% decrease in tumor attenuation of metastatic colorectal liver lesions, measured at pre- and posttreatment portal venous phase multidetector CT, may serve as a surrogate marker of early response in the evaluation after ^{90}Y radioembolization treatment. It is important to emphasize that a mean attenuation value for all voxels included in the lesion must be calculated and that results with high standard deviations in Hounsfield units may affect the confidence of this method. At contrast-enhanced multidetector CT, post-TARE coagulative necrosis appears as an area with a less than 10-HU change in attenuation, indicating the absence of enhancement (6,35). Hence, changes in lesion attenuation or signal intensity must be taken into account when evaluating the response to treatment.

Chun et al (36) described qualitative morphologic CT criteria for predicting response to chemotherapy involving the use of bevacizumab in patients with colorectal liver metastases. With these criteria, lesions are grouped into three pattern categories. These three pattern groups are based on the overall lesion attenuation, tumor-liver interface, and peripheral rim of enhancement. They found that metastases that had heterogeneous attenuation and a thick, poorly defined tumor-liver interface and that became homogeneous in attenuation, with a thin, sharply defined tumor-liver interface after treatment, were well-responding lesions independently of their size. In our experience, some of these criteria could be extrapolated to TARE posttreatment evaluation.

In clinical practice, the most frequent scenario after treatment is the presence of variable areas of necrosis mixed with residual enhancement in many of the lesions, as opposed to complete necrosis of all treated lesions (Table 1). Such changes are often seen during the first 30–45 days and may persist for 2 months. These findings do not have a

Table 1: Imaging Findings Favoring Good Tumor Response after TARE

Response Criteria Used	Findings
mRECIST	Complete response: 100% devascularization
	Partial response: >30% decrease in sum of enhancing viable tumor diameters
Choi	10% reduction in tumor size
	15% reduction in tumor attenuation at portal venous phase multidetector CT
Morphologic	Homogeneous attenuation or signal intensity of treated lesion
	Well-defined tumor-liver interface
	Ring enhancement
Functional	Increased ADC of treated lesion at DW imaging
	Reduced FDG uptake in treated lesion at PET/CT

Note.—ADC = apparent diffusion coefficient, DW = diffusion-weighted.

predictive value if they are present during the early follow-up after TARE. However, persistence after 90 days, especially with arterial phase enhancement, most likely represents residual disease (6). In a review of imaging findings in patients with HCC who were treated with TARE, Mora et al (37) reported persistent enhancement at 1-month follow up in 32 patients, 20 (62%) of whom had complete resolution at 3-month follow-up and no local disease progression at subsequent follow-up imaging. This persistent finding at early follow-up may be due to delayed necrosis (37,38).

Diffusion-weighted Imaging

Beyond the measurement of size and anatomic changes in treated lesions, functional imaging techniques such as diffusion-weighted imaging may have an important role in the assessment of treatment response. Rhee et al (39) reported that diffusion-weighted imaging may aid in early determination of the response to or failure of TARE in patients with HCC (Fig 10) (5).

It may take 2–3 months before tumor size changes are observable with cross-sectional imaging methods; however, early response can be assessed by using diffusion-weighted imaging. The ADCs of responding primary tumors and liver metastases increase after treatment, reflecting a decrease in tumor cellularity.

Diffusion-weighted imaging is useful for evaluating treatment response in hypovascular metastases, in which contrast enhancement representing residual tumor is more difficult to assess. Results of the Barabasch et al study (12) indicate that diffusion-weighted MRI appears to be superior to PET/CT for early assessment of treatment response in patients with hepatic metastases of common solid tumors such as colorectal and breast cancers.

FDG PET/CT

FDG PET is a functional metabolic imaging method with which treatment response is assessed by quantifying the metabolic activity within the tumor as an indicator of tumor viability. The tissue glucose metabolism level can be objectively measured by using semiquantitative parameters such as the standardized uptake value. A decrease in metabolic activity corresponds to tumor response, and conversely, an increase in radiotracer uptake or the presence of new lesions indicates tumor progression. However, owing to the variable FDG avidity in different tumors and tumor differentiation grade, FDG PET is useful only when increased uptake is visualized at pretreatment PET/CT.

Although reduced FDG uptake after radioembolization therapy is well described in the literature as a marker of good response, FDG PET/CT is not routinely used for TARE follow-up because it is more expensive than CT and MRI (6). On the other hand, PET/CT has been found to be valuable for differentiating residual viable neoplastic tissue from benign posttherapy findings such as edema, hemorrhage, and fibrosis (6).

We recommend acquiring a cross-sectional contrast-enhanced image (ie, triphasic CT or diffusion-weighted MR image) 45 days after treatment to assess for complications or progression, and at 3-month intervals after the first posttreatment imaging examination to evaluate treatment response. PET/CT is reserved for use as a problem-solving technique when CT or MRI results are inconclusive.

Perilesional Posttreatment Findings

Imaging after TARE reveals changes in the appearance of the surrounding liver parenchyma as well as the surrounding liver. Important perilesional posttreatment changes are described in Table 2.

Edema and Inflammation

Edema and inflammation are frequent after TARE, and although no definitive pathologic explanation for them has been identified, they are presumably inflammatory reactions to the irradiation (6). Edema and inflammation can appear around the treated lesion or in a perivascular distribution, and they may induce apparent lesion

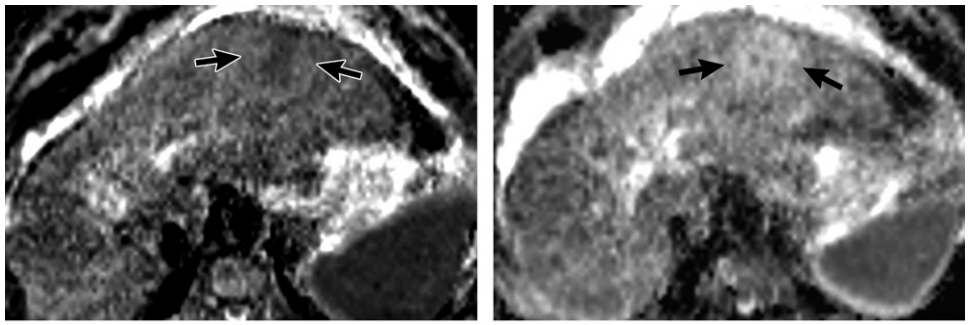

a. b.

Figure 10. Diffusion-weighted imaging evaluation of the response of left lateral segment HCC to TARE in a 66-year-old man. **(a)** Axial pretreatment ADC map of the HCC lesion shows areas of restricted diffusion (arrows). **(b)** Axial early post-TARE follow-up ADC map shows areas of increased ADC (arrows) without areas of restricted diffusion, indicating decreased tumor cellularity.

Table 2: Perilesional Posttreatment Findings

Edema	Ill-defined geographic areas of hypoattenuation at CT or low-signal- intensity areas at MRI during portal venous phase
Inflammation	Areas of increased parenchymal enhancement with ill-defined margins around the treated lesion during arterial and/or portal venous phase
Ring enhancement	Thin rim of enhancement that is usually less than 5 mm in thickness circumscribing the treated lesion
Hepatic fibrosis	Atrophy of the treated lobe with contralateral lobar hypertrophy
Capsular retraction	Retraction of liver capsule
Biliary necrosis and biloma	Small cystic structures usually in clusters around the treated tumor or adjacent to a portal venous branch
Hepatic abscess	May originate as an infected biloma or a necrotic tumor; more common in incompetent ampulla of Vater
REILD	Hepatomegaly with heterogeneous parenchymal enhancement and randomly distributed ill-defined hypoattenuating or hypointense areas in portal venous phase, usually associated with development of ascites

enlargement and disease progression if the assessment is made on the basis of lesion size only (8).

In approximately 40% of treated patients, the perivascular pattern in a previously normal liver parenchyma can appear as ill-defined geographic areas of hypoattenuation at CT or as low-signal-intensity areas at MRI during the portal venous phase (Fig 11). No mass effect is seen, and blood vessels can traverse these areas without distortion (6). Areas with this pattern usually correspond to the vascular territory of a treated segment or lobe. Although this finding has no clinical significance, when it is marked, it may mimic disease progression because its presence in the liver background makes assessment of tumor response more challenging. A peritumoral pattern appears as areas of increased parenchymal enhancement with ill-defined margins around the treated lesion during the arterial or portal venous phase.

Post-TARE inflammatory changes can be distinguished from viable tumor by using diffusion-weighted imaging because inflamed tissue allows free movement of water molecules, which causes attenuation of the diffusion-weighted imaging signal at high *b* values and a highly intense signal on ADC maps. In contrast, viable tumor shows restricted diffusion without signal attenuation at high *b* values

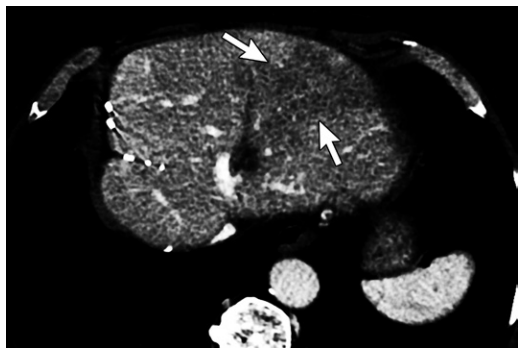

Figure 11. Perivascular edema and inflammation in a 73-year-old man with colorectal liver metastases. Axial portal venous phase MR image obtained after TARE shows ill-defined geographic areas of hypoattenuation with no mass effect (arrows). Note the small blood vessels traversing these areas.

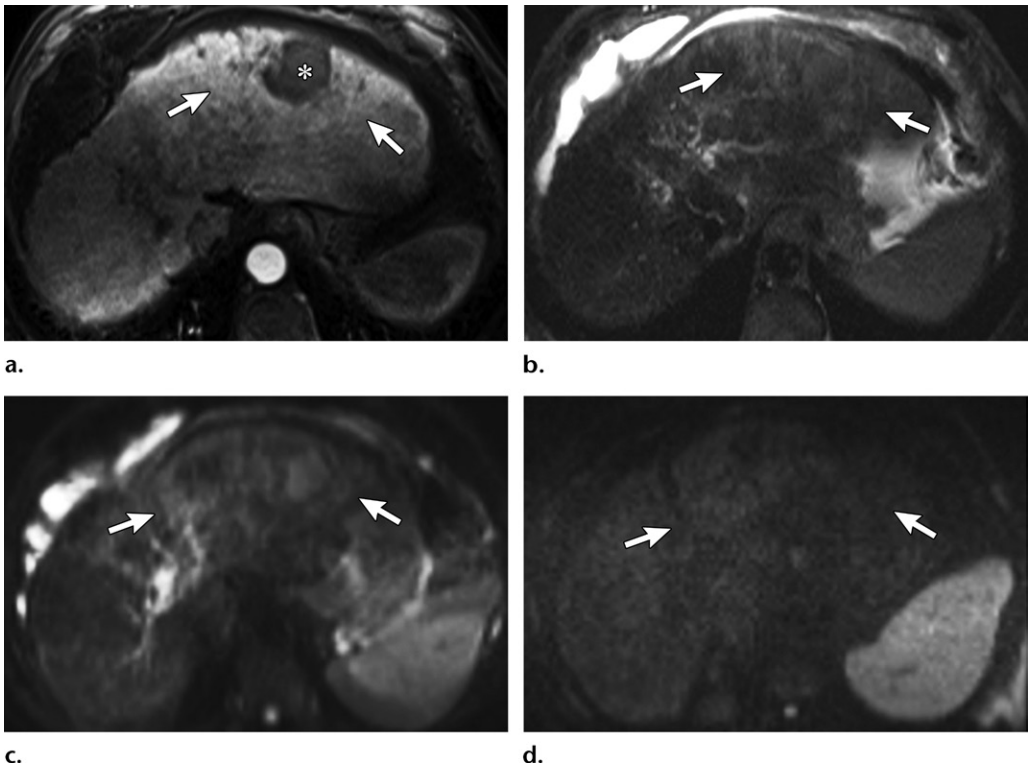

Figure 12. Post-TARE inflammatory changes in a 66-year-old man with HCC. **(a)** Axial posttreatment arterial phase MR image shows ill-defined areas of perilesional parenchymal enhancement (arrows). * = tumor. **(b, c)** Axial T2-weighted fat-saturated **(b)** and diffusion-weighted (b = 50 sec/mm^2) **(c)** MR images show mildly high signal intensity in the treated nontumoral areas (arrows). **(d)** Axial diffusion-weighted (b = 800 sec/mm^2) image shows complete attenuation of the signal, which is isointense to the background parenchyma (arrows). These findings favor benign changes.

and low signal intensity on ADC maps. Although inflammatory changes are transient, they can still be seen 3–6 months after treatment (Fig 12).

Ring Enhancement

A thin rim of enhancement that is usually less than 5 mm in thickness circumscribing a treated lesion is a common finding after TARE that can be seen in about one-third of treated lesions. Keppke et al (35) described this finding in 32% of their procedures. Smooth and uniform rim enhancement usually represents granulation tissue around the tumor as it undergoes radiation necrosis. This rim enhancement may persist for months and does not necessarily imply residual tumor. Kulik et al (40) observed a high correlation between the radiologic finding of peripheral ring enhancement and complete pathologic necrosis of the tumor in specimens explanted from 20 patients with HCC who underwent TARE for bridging or downstaging to resection or transplantation (Fig 13). Thus, complete peritumoral ring enhancement after TARE is indicative of a good response with no viable tumor.

On the other hand, enhancing peripheral nodules represent residual viable tumor, which can result from irregular distribution of the microspheres within the lesions. Many cases of nodular enhancement represent incompletely treated tumors that are in the marginal area between two vascular distributions (35).

Hepatic Fibrosis and Portal Hypertension

Morphologic changes in the liver can occur after TARE, especially in patients who are treated for liver metastases. These changes include atrophy of the treated lobe with contralateral lobar hypertrophy, increased splenic volume, and decreased portal vein diameter (Figs 14, 15) (41). Although radioembolization may cause imaging criteria–based portal hypertension, clinically significant manifestations of portal hypertension such as reduced platelet count (<100 000/dL) and variceal bleeding are rarely seen following the procedure (6,11).

In patients who undergo unilobar TARE, the caliber of the portal vein in the treated lobe may decrease, with an increase in contralateral intrahepatic portal vein diameter and no changes in splenic vein diameter. These findings may be due to fibrosis and remodeling of the treated liver. Irradiation and embolization of vessels cause atrophy of the treated lobes, while, as a compensatory phenomenon induced by variations in

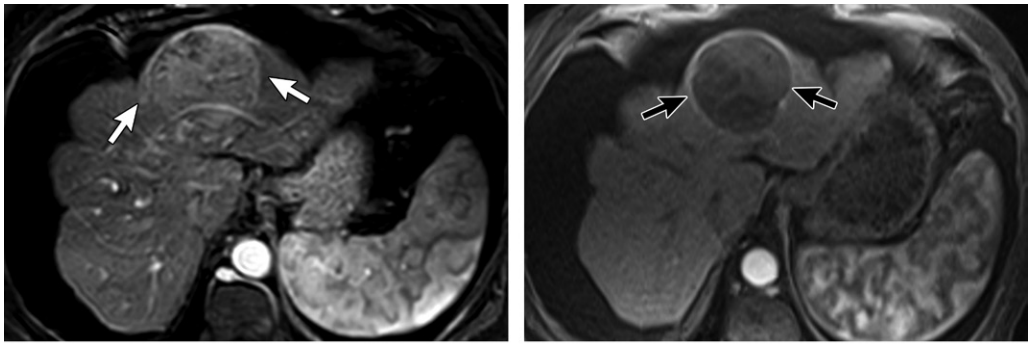

a. b.

Figure 13. Ring enhancement in a 73-year-old woman with HCC. **(a)** Axial pretreatment arterial phase MR image shows HCC (arrows) in the left liver lobe. **(b)** Axial post-TARE arterial phase follow-up MR image shows that the lesion is stable in size but with complete necrosis and ring enhancement (arrows), indicating a complete radiologic response.

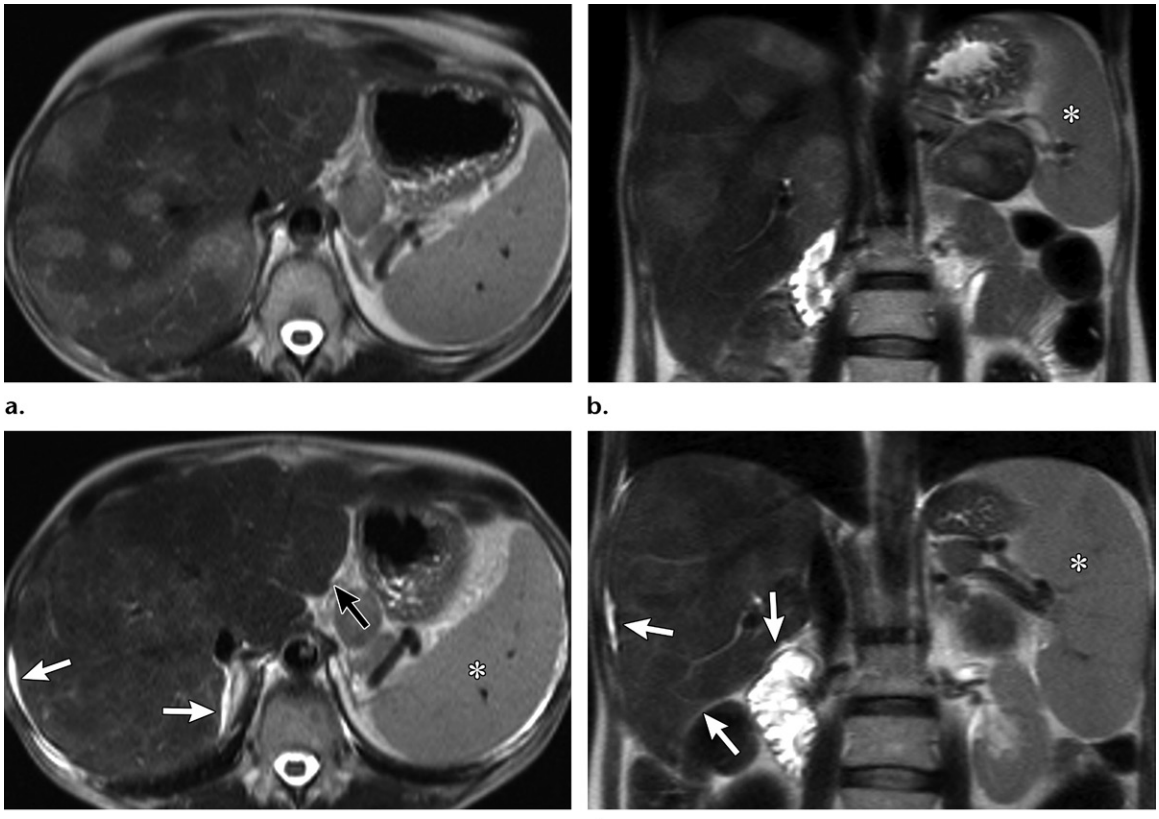

a. b. c. d.

Figure 14. Fibrosis and portal hypertension in a 43-year-old woman with liver metastases from a neuroendocrine tumor. **(a, b)** Axial **(a)** and coronal **(b)** T2-weighted pretreatment MR images show multiple liver metastases. Note the normal size of the spleen (∗ in **b**). **(c, d)** Axial **(c)** and coronal **(d)** T2-weighted post-TARE MR images show reduced lesion size and lobulation of the right lobe (white arrows), with mild enlargement of the left lobe (black arrow in **a**). Splenomegaly (∗), a manifestation of portal hypertension, also is seen.

blood flow, hypertrophy of the contralateral lobe develops (6,11).

In a systematic review of contralateral liver lobe hypertrophy after unilobar ^{90}Y TARE, Teo et al (38) observed contralateral liver hypertrophy ranging from 26% to 47% 44 days to 9 months after the treatment. The rate of hypertrophy after TARE seems to be slower than that associated with other embolization methods. However, we suggest that this procedure constitutes another option in the multidisciplinary management of liver tumors, with the potential to facilitate increased resectability rates, as it can lead to tumor downstaging and future liver remnant hypertrophy.

Superselective intensified radioembolization, also called radiation segmentectomy, is an alternative to surgical resection of some tumors. An

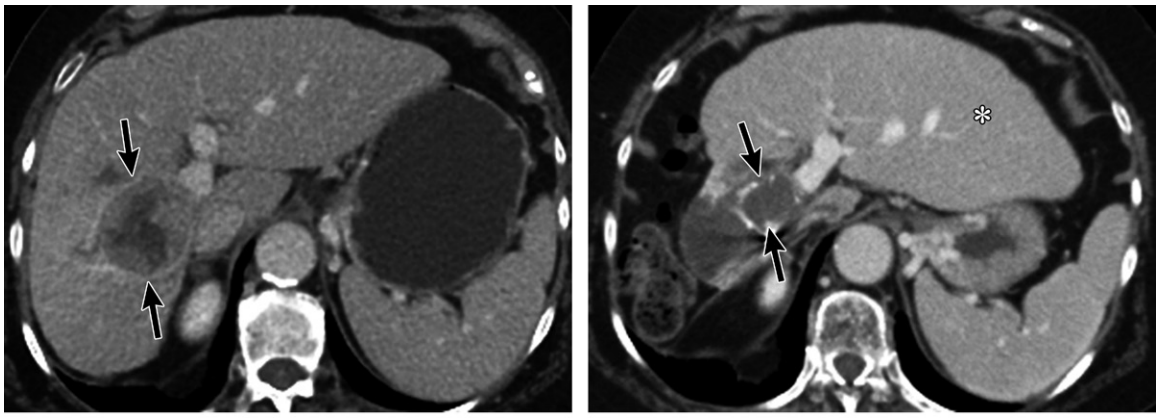

Figure 15. Morphologic changes after TARE in a 51-year-old woman with HCC. **(a)** Axial pretreatment portal venous phase CT image shows HCC (arrows) in the right liver lobe. **(b)** Axial post-TARE portal venous phase follow-up CT image shows a complete response of the treated lesion (arrows), with marked atrophy of the treated lobe and contralateral lobar hypertrophy (*).

ablative radiation dose of up to 1000 Gy can be safely delivered to one segment to induce complete tumor necrosis with capsule retraction and atrophy of the treated segment (Fig 16) (10,37).

Capsular Retraction

In cases of diffuse multifocal disease, the capsular retraction caused by TARE can mimic cirrhosis in an otherwise noncirrhotic liver (Fig 17). This results from necrosis within the tumor that distorts the tumor margin and secondarily the liver capsule, or from an irradiation effect on the liver parenchyma, causing fibrosis and cicatrization (8).

Possible Hepatic Complications

TARE is associated with low toxicity. Lee et al (5) note that according to the Nuclear Regulatory Commission contact scenario, patients in whom less than 3 GBq of activity has been deposited can be released without contact restrictions. However, although radioembolization is generally well tolerated, it may cause relevant toxic effects, including liver injury (42).

Biliary Necrosis and Biloma

Postradioembolization biliary complications are potential side effects of TARE and include biliary dilatation, biloma, and cholangitis (Fig 18). These complications may be due to microvascular occlusion or radiation-induced injury to the biliary system (11). Unlike the hepatic parenchyma, which has a dual blood supply, the biliary tree is irrigated by the peribiliary plexus only. The blood vessels that constitute the peribiliary plexus are 20–60 μm in diameter. This vessel diameter enables the 20–40-mm microspheres used in TARE to become trapped and cause both ischemia and radiation-induced biliary necrosis. This process explains the susceptibility of the biliary tree to ischemic injury after transarterial therapies in the liver (6). The incidence of these complications is less than 10% (43).

Compared with noncirrhotic livers, cirrhotic livers have hypertrophy of the peribiliary plexus and thus a lower risk of biliary necrosis after radioembolization. Acute biliary necrosis is seen as small cystic structures within the distribution of an embolized artery, adjacent to a portal venous branch. They are usually in clusters around a treated tumor. These structures can rupture, leaking bile and causing coagulation necrosis of the adjacent hepatic parenchyma and thrombosis of the small arterial vessels in the vicinity. The leaking bile accumulates to form a biloma (6). Similar findings have been described in association with other procedures such as transarterial chemoembolization performed with drug-eluting beads (44,45).

Peripheral enhancement around a biloma is seen frequently and does not always imply infection. Bile duct stenosis and dilatation indicate chronic injury. Most biliary complications are asymptomatic and require no treatment (6).

Hepatic Abscess

Microorganisms get to the hepatic parenchyma by means of ascending cholangitis, chronic biliary colonization, or portal pyemia; abscesses are more frequent in patients with an incompetent ampulla of Vater (eg, bilioenteric anastomosis). A hepatic abscess can originate as infection of either a biloma or necrotic tumor (6). Clinical manifestations of a liver abscess typically are right upper quadrant abdominal pain, right shoulder pain, nausea, vomiting, fever and chills, chest pain, shortness of breath, and in some patients, cough and weight loss (6,8).

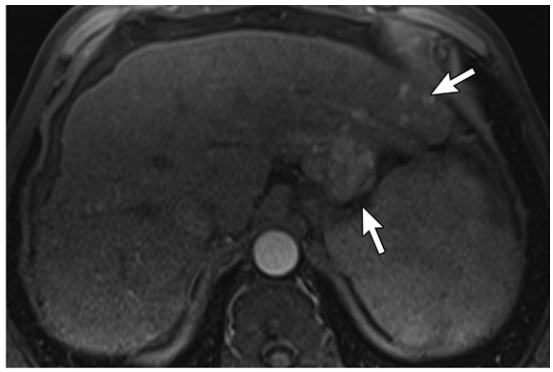

a.

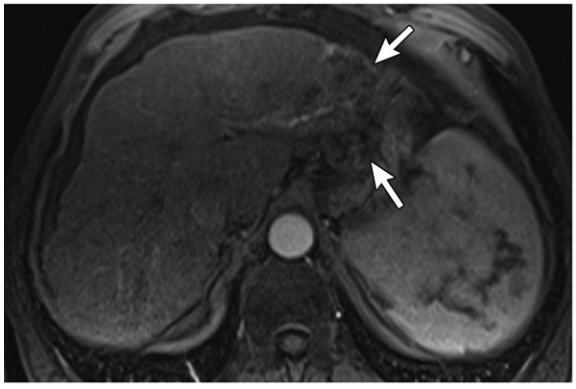

b.

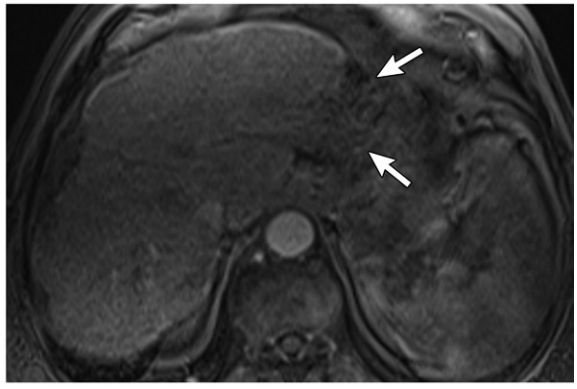

c.

Figure 16. Complete tumor response to radiation segmentectomy in a 55-year-old man. **(a)** Axial pretreatment arterial phase MR image shows multiple HCCs (arrows) in liver segments II and III. **(b, c)** Axial arterial phase follow-up MR images obtained 3 months **(b)** and 6 months **(c)** after TARE show reduced size and devascularization of the treated lesions (arrows), with complete atrophy of the left lateral segment.

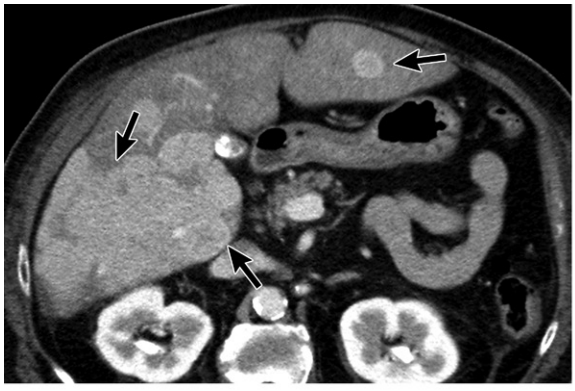

a.

b.

Figure 17. Capsular retraction in a 71-year-old man with HCC. **(a)** Axial pretreatment arterial phase CT image shows multiple HCC lesions (arrows). **(b)** Axial post-TARE arterial phase follow-up CT image shows a complete response of the treated lesion in liver segment III and devascularization with necrotic changes in the right lobe lesions (black arrows). Also note the marked liver surface irregularity, with capsular retraction and atrophy of the posterior right lobe (white arrows).

Radioembolization-induced Liver Disease

REILD is potentially life-threatening liver damage that is characterized by jaundice and ascites that develop 4–8 weeks after treatment. It is more frequently observed after bilobar (sequential) treatments. The overall incidence of REILD after TARE ranges from 4% to 9% (6). However, in patients who have undergone pretreatment with chemotherapeutic agents, the incidence can reach up to 20% (40).

REILD should be studied within the spectrum of sinusoidal obstruction syndromes, external radiation-induced liver disease, and liver disease in patients who undergo allogeneic bone marrow transplant (42,46). Affected patients have increased total bilirubin, alkaline phosphatase, and γ-glutamyl transpeptidase levels, with no changes in transaminase levels and without obvious biliary dilatation or tumor progression (6). Pathologic changes are consistent with veno-occlusive disease and include extensive sinusoidal congestion in perivenular areas with focal hepatic atrophy, areas of necrosis around central veins with fresh thrombosis, and cholestasis in periportal areas (42).

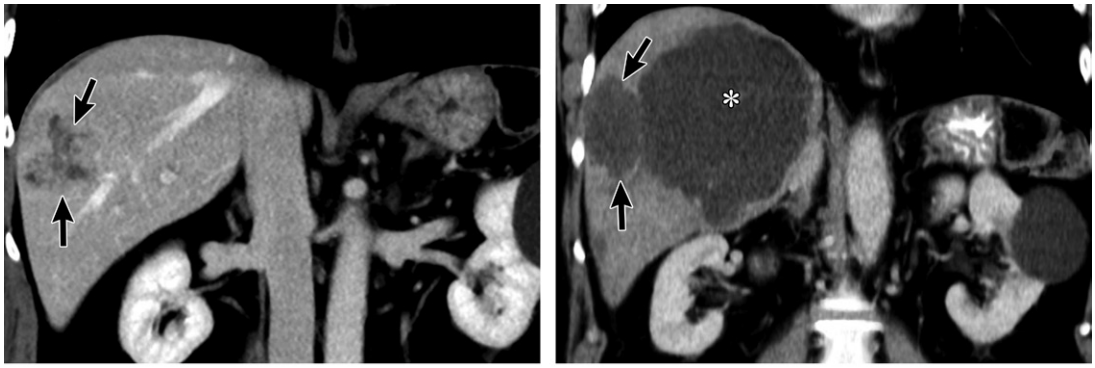

a. b.

Figure 18. Biloma in a 70-year-old man with a metastatic neuroendocrine tumor. **(a)** Coronal pretreatment portal venous phase CT image shows the metastatic lesion (arrows). **(b)** Coronal post-TARE portal venous phase follow-up CT image shows a complete response of the treated lesion (arrows). Also note the large well-defined fluid-filled area (*) adjacent to the lesion, representing a biloma.

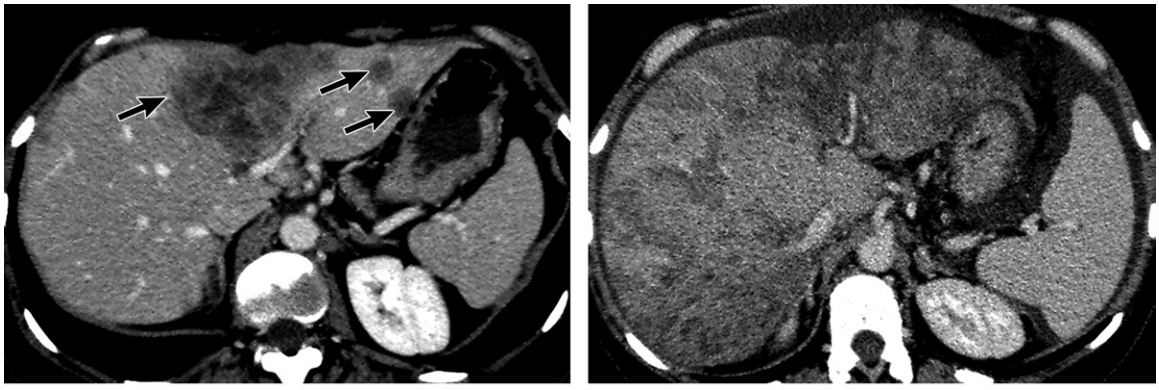

a. b.

Figure 19. REILD in a 42-year-old woman with metastatic breast cancer. **(a)** Axial portal venous phase CT image shows liver metastases (arrows) in the left lobe. **(b)** Axial post-TARE follow-up CT image shows hepatomegaly, with marked parenchymal heterogeneity and ill-defined hypoattenuating areas in both lobes. Ascites and mild splenomegaly also are seen.

Radiologic findings are nonspecific and include hepatomegaly with heterogeneous parenchymal enhancement and ill-defined hypoattenuating or hypointense areas randomly distributed during the portal venous phase, usually in association with the development of ascites (Fig 19). The diagnosis is determined by taking into account the clinical scenario and laboratory test results. Imaging studies have an important role in excluding tumor progression and other diagnoses associated with the symptoms (eg, biliary stones) (6).

Extrahepatic Findings and Complications

Radiation-induced Cholecystitis

Typical radiologic findings include an edematous and enhancing gallbladder wall, which can occasionally show disruption. Pericholecystic fluid also can be found. This complication can be prevented by identifying the cystic artery and delivering microspheres distal to its origin (11). Unlike in the setting of non–radiation-induced cholecystitis, with radiation-induced cholecystitis, if the patient is well clinically, radiologic evidence of acute cholecystitis, even if it is complicated, does not require active surgical management. Fewer than 1% of patients with radiation-induced cholecystitis require surgical intervention (6,43).

Perihepatic Fluid and Pleural Effusion

Although most microspheres are delivered to targeted areas, some amount of irradiation of extrahepatic structures such as the Glisson capsule and the right pleural space may result in reactive perihepatic fluid and pleural effusions, most frequently after right lobe procedures (8). These effusions are usually self-limiting and require only the treatment of symptoms, if these are present (6).

Gastrointestinal Complications

Gastrointestinal complications occur as a result of the aberrant deposition of microspheres into the gastrointestinal tract, which is caused by the

presence of nondetected hepaticoenteric arterial communications. The incidence of these complications is less than 5% (11).

Radiation Pneumonitis

Radiation pneumonitis associated with TARE is rare, with an incidence of less than 1%, provided proper lung shunting studies and dosimetry are performed. The pathophysiology of this phenomenon involves a shunt between the hepatic arterial circulation and the pulmonary circulation (10,11). This happens when there is an intratumoral shunt between the hepatic artery and hepatic veins. Radiologically, radiation pneumonitis manifests 1–2 months after therapy as ill-defined patchy opacities and ground-glass opacities in a symmetric pattern, with relative hilar or perihilar sparing (6) (Fig 20).

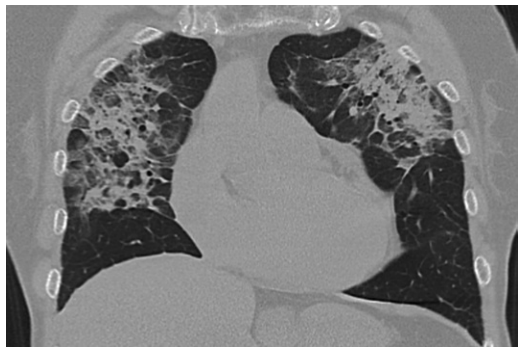

Figure 20. Radiation pneumonitis in a 62-year-old woman with HCC. Coronal CT image of the lungs after TARE shows ill-defined areas of consolidation and ground-glass opacities in a symmetric pattern, with relative hilar or perihilar sparing.

Radiation Dermatitis

Radiation dermatitis occurs when microspheres are delivered to the anterior abdominal wall through the falciform artery. It manifests as periumbilical pain (6,11). Recognition of the falciform artery is needed to prevent this complication. The falciform artery usually arises from arteries supplying liver segments IV (68%) and III, and common trunk segments II and III. It runs in the falciform ligament along the paraumbilical vein and then spreads out around the umbilicus and communicates with the distal branches of the superior and inferior epigastric arteries (3). Topically applying ice prevents complications by causing vasoconstriction, which decreases cutaneous flow (3).

Conclusion

TARE is an interventional radiology technique used to treat primary liver tumors and liver metastases. A multidisciplinary team is necessary to ensure optimal results. Clinical success depends on the correct selection of patients and can be achieved with complete pretreatment planning. This planning must include a simulating phase to detect excessive hepatopulmonary shunting and identify vessels that could deliver microspheres to nontargeted organs.

Despite all precautions, some degree of irradiation of the normal liver parenchyma may occur and induce many lesional and perilesional changes that can differ from those seen with other therapeutic procedures. Radiologists must be familiar with the spectrum of these changes to avoid misinterpreting them as disease progression, which might affect patient treatment. Finally, it is important to recognize that the goal in performing TARE is to induce tumor necrosis with size reduction; however, the treatment response is time dependent and can take 3–6 months to become evident.

References

1. Herba MJ, Illescas FF, Thirlwell MP, et al. Hepatic malignancies: improved treatment with intraarterial Y-90. Radiology 1988;169(2):311–314.
2. Salem R, Lewandowski RJ, Sato KT, et al. Technical aspects of radioembolization with 90Y microspheres. Tech Vasc Interv Radiol 2007;10(1):12–29.
3. Vesselle G, Petit I, Boucebci S, Rocher T, Velasco S, Tasu JP. Radioembolization with yttrium-90 microspheres work up: practical approach and literature review. Diagn Interv Imaging 2015;96(6):547–562.
4. Uliel L, Royal HD, Darcy MD, Zuckerman DA, Sharma A, Saad NE. From the angio suite to the γ-camera: vascular mapping and 99mTc-MAA hepatic perfusion imaging before liver radioembolization—a comprehensive pictorial review. J Nucl Med 2012;53(11):1736–1747.
5. Lee EW, Alanis L, Cho S-K, Saab S. Yttrium-90 selective internal radiation therapy with glass microspheres for hepatocellular carcinoma: current and updated literature review. Korean J Radiol 2016;17(4):472–488.
6. Singh P, Anil G. Yttrium-90 radioembolization of liver tumors: what do the images tell us? Cancer Imaging 2014;13(4):645–657.
7. Peker A, Çiçek O, Soydal Ç, Küçük NÖ, Bilgiç S. Radioembolization with yttrium-90 resin microspheres for neuroendocrine tumor liver metastases. Diagn Interv Radiol 2015;21(1):54–59.
8. Atassi B, Bangash AK, Bahrani A, et al. Multimodality imaging following 90Y radioembolization: a comprehensive review and pictorial essay. RadioGraphics 2008;28(1):81–99.
9. Tochetto SM, Töre HG, Chalian H, Yaghmai V. Colorectal liver metastasis after 90Y radioembolization therapy: pilot study of change in MDCT attenuation as a surrogate marker for future FDG PET response. AJR Am J Roentgenol 2012;198(5):1093–1099.
10. Kim HC. Radioembolization for the treatment of hepatocellular carcinoma. Clin Mol Hepatol 2017;23 (2):109–114.
11. Riaz A, Awais R, Salem R. Side effects of yttrium-90 radioembolization. Front Oncol 2014;4:198.
12. Barabasch A, Kraemer NA, Ciritsis A, et al. Diagnostic accuracy of diffusion-weighted magnetic resonance imaging versus positron emission tomography/computed tomography for early response assessment of liver metastases to Y90-radioembolization. Invest Radiol 2015;50(6):409–415.
13. Kao YH, Hock Tan AE, Burgmans MC, et al. Image-guided personalized predictive dosimetry by artery-specific SPECT/CT partition modeling for safe and effective 90Y radioembolization. J Nucl Med 2012;53(4):559–566.
14. Sangro B, Iñarrairaegui M, Bilbao JI. Radioembolization for hepatocellular carcinoma. J Hepatol 2012;56(2):464–473.

15. Giammarile F, Bodei L, Chiesa C, et al. EANM procedure guideline for the treatment of liver cancer and liver metastases with intra-arterial radioactive compounds. Eur J Nucl Med Mol Imaging 2011;38(7):1393–1406.
16. Lambert B, Mertens J, Sturm EJ, Stienaers S, Defreyne L, D'Asseler Y. 99mTc-labelled macroaggregated albumin (MAA) scintigraphy for planning treatment with 90Y microspheres. Eur J Nucl Med Mol Imaging 2010;37(12):2328–2333.
17. Sabet A, Ahmadzadehfar H, Muckle M, et al. Significance of oral administration of sodium perchlorate in planning liver-directed radioembolization. J Nucl Med 2011;52(7): 1063–1067.
18. Ahmadzadehfar H, Sabet A, Biermann K, et al. The significance of 99mTc-MAA SPECT/CT liver perfusion imaging in treatment planning for 90Y-microsphere selective internal radiation treatment. J Nucl Med 2010;51(8):1206–1212.
19. Ahmadzadehfar H, Biersack HJ, Ezziddin S. Radioembolization of liver tumors with yttrium-90 microspheres. Semin Nucl Med 2010;40(2):105–121.
20. Sirtex medical training manual. http://www.sirtex.com/eu/clinicians/package-insert/. Accessed January 14, 2015.
21. Langsteger W. EANM 2011: welcome to Birmingham! Eur J Nucl Med Mol Imaging 2011;38(suppl 2):79.
22. Hamami ME, Poeppel TD, Müller S, et al. SPECT/CT with 99mTc-MAA in radioembolization with 90Y microspheres in patients with hepatocellular cancer. J Nucl Med 2009;50(5):688–692.
23. Lenoir L, Edeline J, Rolland Y, et al. Usefulness and pitfalls of MAA SPECT/CT in identifying digestive extrahepatic uptake when planning liver radioembolization. Eur J Nucl Med Mol Imaging 2012;39(5):872–880.
24. Gulec SA, Mesoloras G, Stabin M. Dosimetric techniques in 90Y-microsphere therapy of liver cancer: the MIRD equations for dose calculations. J Nucl Med 2006;47(7):1209–1211.
25. Bapst B, Lagadec M, Breguet R, Vilgrain V, Ronot M. Cone beam computed tomography (CBCT) in the field of interventional oncology of the liver. Cardiovasc Intervent Radiol 2016;39(1):8–20. [Published correction appears in Cardiovasc Intervent Radiol 2015;38(5):1381.]
26. Louie JD, Kothary N, Kuo WT, et al. Incorporating cone-beam CT into the treatment planning for yttrium-90 radioembolization. J Vasc Interv Radiol 2009;20(5): 606–613.
27. Ito S, Kurosawa H, Kasahara H, et al. (90)Y bremsstrahlung emission computed tomography using gamma cameras. Ann Nucl Med 2009;23(3):257–267.
28. Lhommel R, van Elmbt L, Goffette P, et al. Feasibility of 90Y TOF PET-based dosimetry in liver metastasis therapy using SIR-Spheres. Eur J Nucl Med Mol Imaging 2010;37(9):1654–1662.
29. Willowson KP, Tapner M; QUEST Investigator Team, Bailey DL. A multicentre comparison of quantitative (90) Y PET/CT for dosimetric purposes after radioembolization with resin microspheres: the QUEST Phantom Study. Eur J Nucl Med Mol Imaging 2015;42(8):1202–1222.
30. Fournier L, Ammari S, Thiam R, Cuénod CA. Imaging criteria for assessing tumour response: RECIST, mRECIST, Cheson. Diagn Interv Imaging 2014;95(7-8):689–703.
31. Lencioni R, Llovet JM. Modified RECIST (mRECIST) assessment for hepatocellular carcinoma. Semin Liver Dis 2010;30(1):52–60.
32. Choi H, Charnsangavej C, de Castro Faria S, et al. CT evaluation of the response of gastrointestinal stromal tumors after imatinib mesylate treatment: a quantitative analysis correlated with FDG PET findings. AJR Am J Roentgenol 2004;183(6):1619–1628.
33. Weng Z, Ertle J, Zheng S, et al. Choi criteria are superior in evaluating tumor response in patients treated with transarterial radioembolization for hepatocellular carcinoma. Oncol Lett 2013;6(6):1707–1712.
34. Eisenhauer EA, Therasse P, Bogaerts J, et al. New response evaluation criteria in solid tumours: revised RECIST guideline (version 1.1). Eur J Cancer 2009;45(2):228–247.
35. Keppke AL, Salem R, Reddy D, et al. Imaging of hepatocellular carcinoma after treatment with yttrium-90 microspheres. AJR Am J Roentgenol 2007;188(3):768–775.
36. Chun YS, Vauthey JN, Boonsirikamchai P, et al. Association of computed tomography morphologic criteria with pathologic response and survival in patients treated with bevacizumab for colorectal liver metastases. JAMA 2009;302(21):2338–2344.
37. Mora RA, Ali R, Gabr A, et al. Pictorial essay: imaging findings following Y90 radiation segmentectomy for hepatocellular carcinoma. Abdom Radiol (NY) 2017; 43(7):1723–1738.
38. Teo JY, Allen JC Jr, Ng DC, et al. A systematic review of contralateral liver lobe hypertrophy after unilobar selective internal radiation therapy with Y90. HPB (Oxford) 2016;18(1):7–12.
39. Rhee TK, Naik NK, Deng J, et al. Tumor response after yttrium-90 radioembolization for hepatocellular carcinoma: comparison of diffusion-weighted functional MR imaging with anatomic MR imaging. J Vasc Interv Radiol 2008;19(8):1180–1186.
40. Kulik LM, Atassi B, van Holsbeeck L, et al. Yttrium-90 microspheres (TheraSphere) treatment of unresectable hepatocellular carcinoma: downstaging to resection, RFA and bridge to transplantation. J Surg Oncol 2006;94(7):572–586.
41. Jakobs TF, Saleem S, Atassi B, et al. Fibrosis, portal hypertension, and hepatic volume changes induced by intra-arterial radiotherapy with 90yttrium microspheres. Dig Dis Sci 2008;53(9):2556–2563.
42. Sangro B, Gil-Alzugaray B, Rodriguez J, et al. Liver disease induced by radioembolization of liver tumors: description and possible risk factors. Cancer 2008;112(7):1538–1546.
43. Atassi B, Bangash AK, Lewandowski RJ, et al. Biliary sequelae following radioembolization with yttrium-90 microspheres. J Vasc Interv Radiol 2008;19(5):691–697.
44. Guiu B, Deschamps F, Aho S, et al. Liver/biliary injuries following chemoembolisation of endocrine tumours and hepatocellular carcinoma: lipiodol vs drug-eluting beads. J Hepatol 2012;56(3):609–617.
45. Spina JC, Ulla M, Yeyati EL, et al. MDCT findings after hepatic chemoembolization with DC-beads: what the radiologist needs to know. Abdom Imaging 2013;38 (4):778–784.
46. Gil-Alzugaray B, Chopitea A, Iñarrairaegui M, et al. Prognostic factors and prevention of radioembolization-induced liver disease. Hepatology 2013;57(3):1078–1087.